Rugged Linear Array for IoT Applications

Lidong Chi, *Student Member*, *IEEE,* Zi-Bin Weng*, Member, IEEE*, Shu Meng, Yihong Qi, *Senior Member, IEEE*, Jun Fan, *Fellow, IEEE*, Weihua Zhuang, *Fellow, IEEE* , and James Drewniak*, Fellow, IEEEE*

***Abstract*—A rugged linear array is proposed for covering both the LTE and 5G bands with an intermediate gain. The antenna is composed of a driven element, a set of directors, and a set of reflectors, where the excited element is a wideband high-efficiency electromagnetic structure (WHEMS) and the parasitic elements consist of metal rods. To achieve a rugged design, similar to the classic Yagi antenna, all of the elements should be conductively connected, so that it can be welded. The weldable mechanism is started on the driven radiating element. In addition, a voltage balun is introduced in the antenna to reduce the influence of unbalanced common mode currents. A wind resistance analysis is also presented, where the drag force of the proposed antenna is approximately a quarter of that for an antenna with a metal plate. The antenna exhibits a gain of 10.8–13.3 dBi for a 78% fractional bandwidth (1.7–3.7 GHz), which is a 7-fold increase from that of the Yagi antenna, without sacrificing the gain or rugged design. The proposed antenna has the advantages of a simple feeding arrangement, low cost, light weight, low wind resistance, and rugged structure; and is suitable for all-weather large-scale Internet of Things (IoT) deployment on the rural site or in a harsh networking environment.**

***Index Terms*— Linear antenna array, LTE, 5G, WHEMS, Yagi antenna, balun.**

I. Introduction

Currently, the Internet of Things (IoT) is broadly applied in fields such as intelligent transport systems [1], industry 4.0 [2], smart precision agriculture [3], smart hospitals [4], and more [5]-[12]. The development of IoT will provide further advancements and will improve productivity through remote real-time control, monitoring, and diagnosis via the deployment of massive communication nodes with various sensors [13]-[15], which will benefit applications such as smart precision farming in rural areas [16], leak detection for oil and gas pipelines in remote regions [17], remote medical treatment [18], and so forth [19]. Therefore, a substantial number of high-performance, low-cost antennas are needed. In these applications, high-definition video streaming and "zero latency" reactions have led to higher requirements for communication capacity, and for the antennas such as wide-band and high-gain properties [20]-[21]. To meet these requirements, technical advances in LTE and 5G and beyond have been involved in IoT applications [22]-[23]. Considering the need for large-scale deployment and suitability for various types of networking environments, antennas should have the desired characteristics of simplicity, low cost, light weight, low wind resistance, and rugged structure. For example, for the oil field applications, oil and gas pipelines are maintained under extreme working conditions (high wind, high temperature, and high humidity) in the desert and wilderness, where only antennas with rugged structure and low wind load are suitable.

Directional antennas are widely used in the outdoor applications, such as 5G, Sub-6G and point-to-point communications. In the applications, the electric part of the IoT system can be well protected, but the directional antennas are set up high to ensure line-of-sight communication. In theoe circumstances, the antennas are critical and the most fragile part of the IoT system, due to the wind and other environment factors. Therefore, the antenna in outdoor IoT applications should not only be electrically high performance, but also be able to resist strong winds and other harsh environment conditions. Featuring the advantages of a simple feeding arrangement, low cost, light weight, low wind resistance, and rugged structure, the Yagi antenna, which has been found in hundreds of million pieces in the outdoor applications, is an ingenious invention and a competitive candidate for IoT applications [24]- [26]. However, its impedance bandwidth of only 10% largely restricts its applications in IoT [25][27]. Considering LTE, one of the IoT supporting technologies, as an example, five classic Yagi antennas are needed to cover the 45% fractional bandwidth of LTE, with the need for additional antennas to achieve compatibility with other communication systems such as 5G and beyond. This aspect introduces inconvenience and a substantial constraint on inventory and logistics. In addition, from a structural point of view, the end-fire dimension is too large for some IoT applications when the classic Yagi antenna obtains a high gain.

The classic Yagi antenna has gained popularity worldwide since its first description in an English journal in 1926 and has been recently applied in photonics and quantum physics [28]-[30]. Shown in Table I, the quasi-Yagi antenna has an

L. Chi is with Hunan University, Changsha 410082, China, and General Test Systems Inc., Shenzhen 518000, China (e-mail: 565548254@qq.com).

Z. Weng (corresponding author) is with Xidian University, Xi'an 710071, China (e-mail: zibinweng@mail.xidian.edu.cn).

S. Meng is with DBJay Inc., Zhuhai 519000, China (shu.meng@dbjtech.com).

Y. Qi is with Hunan University, Changsha 410006, Chin; General Test Systems, Shenzhen 518102, China; and Missouri University of Science and Technology, Rolla, MO 65409 USA (e-mail: yihong.qi@generaltest.com and yihong.qi@dbjtech.com).

J. Fan is with the EMC Laboratory, Missouri University of Science and Technology, Rolla, MO 65409 USA (e-mail: jfan@mst.edu).

W. Zhuang is with the Department of Electrical and Computer Engineering, University of Waterloo, Waterloo, ON N2L 3G1, Canada (e-mail: wzhuang@uwaterloo.ca).

J. L. Drewniak is with the EMC Laboratory, Missouri University of Science and Technology, Rolla, MO 65401 USA (e-mail: drewniak@mst.edu).

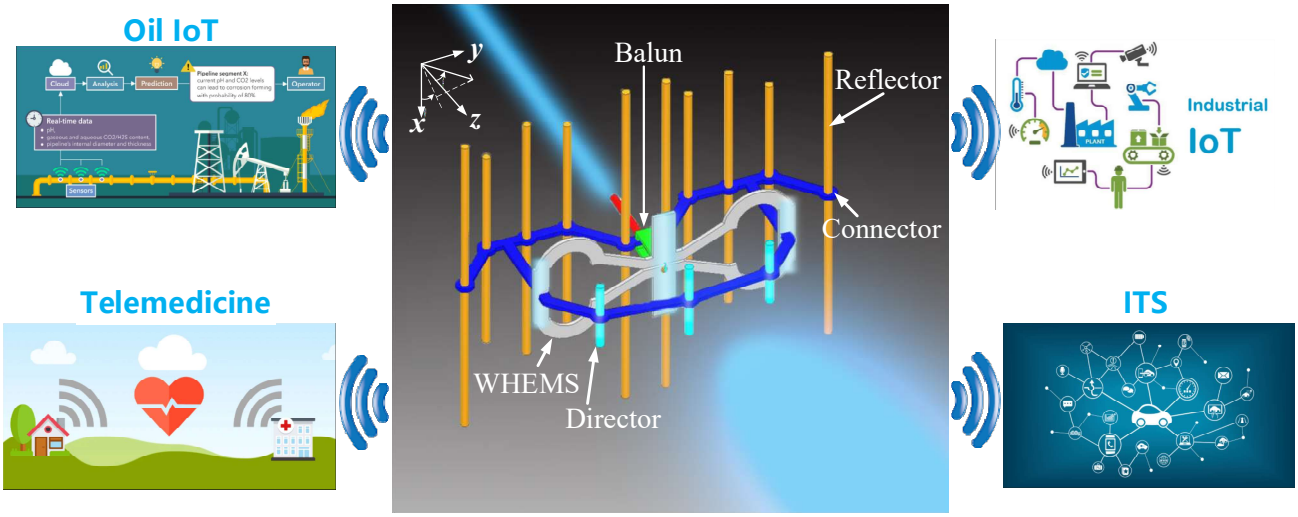

Fig. 1. The proposed antenna with its wide IoT applications.

improved fractional impedance bandwidth of 78% or more; however, the gain is at least 2 dB lower than that of the classic Yagi antenna (with the same number of directors) [31]-[34]. The improvement is achieved via the feeding structures in the printed circuit board (PCB), which is not sufficiently sturdy for outdoor applications [35]. The log-periodic antenna is also a wide-band linear antenna; however, it normally obtains a gain of approximately 8 dBi in the band, with a large end-fire size exceeding the wavelength at its center frequency [36]-[38]. As the log-periodic is not sufficiently rugged, a radome is needed for outdoor applications, which increases the cost, wind load, and weight._Similar to how the classic Yagi antenna brought TV signals to homes worldwide, thanks to its five advantages (simple feeding arrangement, low cost, light weight, low wind resistance, and rugged structure), an antenna with both the advantages of classic Yagi antenna as well as wide-band performance and compact size is needed to bring IoT applications into various sectors in society.

TABLE I

Performance comparision

Ref.	BW.	Gain(dBi)	Dimensions	Processing
[26]	9.90%	6.8	1.0*0.5 λ_L^2	PCB
[31]	20.00%	6.5	0.5*0.5 λ_L^2	PCB
[33]	48.00%	3.0-5.0	0.4*0.4 λ_L^2	PCB
[34]	78.40%	6.4-7.4	7.4*1.0 λ_L^2	PCB
[36]	72.70%	6.0-8.5	0.9*0.4 λ_L^2	PCB
[37]	180.10%	3.0-6.0	0.4*0.4 λ_L^2	PCB
[38]	100.80%	5.3-8.7	2.0*0.6 λ_L^2	PCB
[46]	45.50%	11.0-12.0	0.4*0.9*1.0 λ_L^3	Metal rod
This work	74.00%	10.8-13.3	0.4*1.0*1.2 λ_L^3	Metal rod

The classic Yagi antenna is a linear antenna, which has advantages of low wind resistance and light weight. Consisting of parasitic elements (directors and a reflector) and a driven element, it needs only one feeding point, making it sufficiently simple without a complex feeding network. The rugged

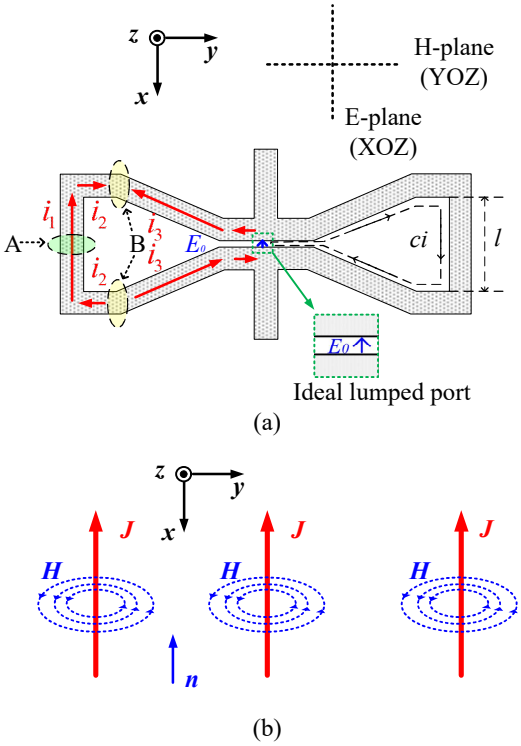

Fig. 2 (a) The current analysis model of the WHEMS antenna. (b) The H-plane equivalent current model of WHEMS.

structure is realized by welding all of the elements together through a long metal rod. Due to its wide-band high-gain characteristics, the wide-band high-efficiency electromagnetic structure (WHEMS) can be applied as the driven element to widen the bandwidth of the classic Yagi antenna [39]-[46]. In [46], it is shown that a rod director is efficient for the WHEMS. However, the plate reflector and the connecting polyester column result in a high wind load and render the antenna less rugged. In this paper, a connection structure is proposed for the linear WHEMS and parasitic rod elements, as illustrated in Fig. 1, which maintain the five advantages of the classic Yagi antenna. Combined with a rugged design, the antenna is intended to cover both the LTE and 5G Sub-6GHz bands,

which makes it suitable for various types of environments in IoT applications.

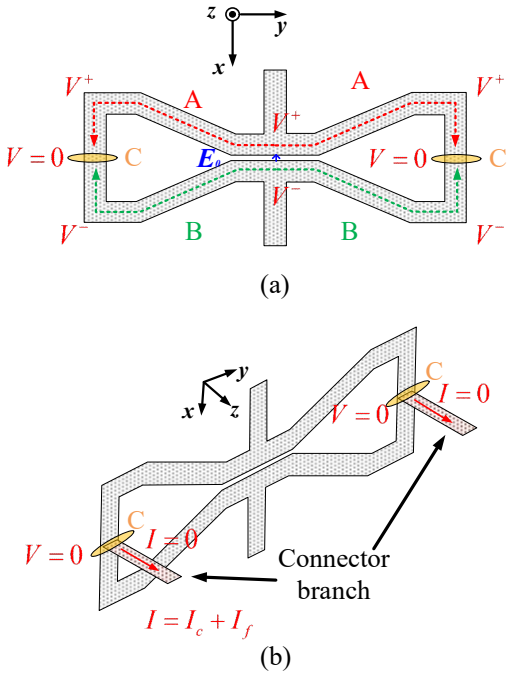

Fig. 3 (a) The voltage analysis of the WHEMS. (b) The current distribution of the connector branch.

In Section II, the radiating mechanism and the equivalent source model of the WHEMS are introduced. Then, the weldability and the wide-band medium/high-gain property of the antenna are discussed, along with the balun. Electromagnetic simulations are presented in Section III, validating the theory in Section II. The wind load is analyzed in Section IV. Subsequently, the simulated and measured numerical results are discussed in Section V, followed by conclusions in Section VI.

II. Theory

In addition to its excellent directional radiating performance, the classic Yagi antenna has gained popularity worldwide due to its primary mechanical advantages, i.e., simple feeding arrangement, low cost, light weight, low wind resistance, and rugged structure, resulting in an all-weather available antenna with convenient installation. These merits arise from its linear array and rugged design, where the antenna consists of metal rods connected by a weldable structure. Our antenna proposed in this work not only inherits the merits of the Yagi antenna, achieved by applying a linear array and welding design, but also realizes an intermediate gain over a wide band, seven-fold wider than that of the classic Yagi antenna. In this section, the radiating mechanism and the equivalent source model of the WHEMS are introduced. Based on the description, the weldability and the wide-band medium/high-gain property are discussed. Finally, a voltage balun is introduced to the WHEMS antenna, which can reduce interference caused by unbalanced common mode currents.

A. Radiating Model

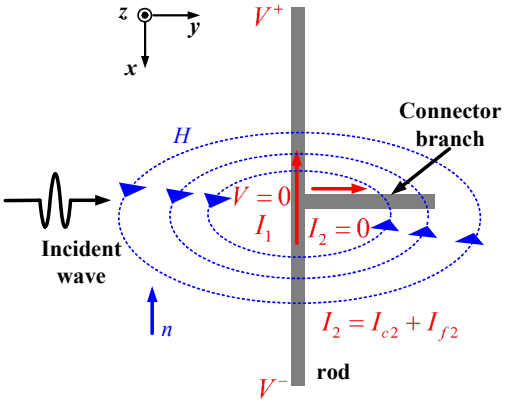

Fig. 4 The voltage and current analysis of the parasitic rod and its connector branch.

The theoretical model of a linear WHEMS is shown in Fig. 2a, where the gray regions represent metal. This antenna is a two-dimensional symmetrical structure with an ideal lumped port in the middle (blue arrow) represented as E_0. Parameters ci and l represent the perimeter of half of the antenna slot and the length of the slot edge, equal to the wavelength and half wavelength, respectively, which are general applied for a WHEMS antenna [43]. The current distribution is also shown. Region A is the short circuit point of the antenna, which is the current crest point. Starting from A, region B is the current trough point when the total length of i_1 and i_2 is half a wavelength. The current changes its flow direction at region B. Based on the superposition principle, the current distribution is equivalent to a three-linear current source in H-plane radiation, as shown in Fig. 2b [46]. The position of region B can change for different frequencies, which in turn changes the phase and amplitude of the linear currents. However, the equivalent current model of the WHEMS remains unchanged as region B moves. Thus, the distribution can be maintained over a wide band, where the amplitude and phase of the equivalent linear currents change with frequency.

The Ampère's law, with Maxwell's addition, is given by

$$\nabla \times H = J + \frac{\partial D}{\partial t} \tag{1}$$

where H, J, and D are the magnetic field strength, electric current density, and dielectric displacement vector, respectively. From (1), ring magnetic fields, as shown in Fig. 1b, are generated by the equivalent linear currents with their normal vector parallel to the x axis.

B. Connection Theory

Fig. 3a shows a front view of the simplified theoretical model of the WHEMS antenna. The antenna is an axisymmetric model with an ideal lumped feeding port precisely in the middle. Excited by the port, voltages V^+ and V^- arise on each side of the gap, which have the same amplitude but a phase difference of 180 degrees. Because the antenna is symmetric, the length of

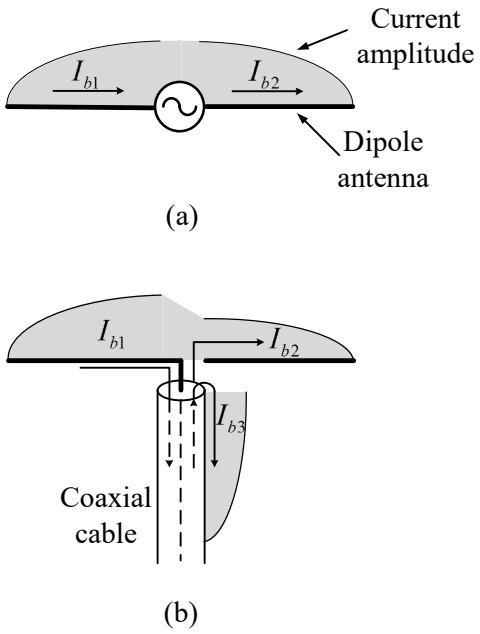

Fig. 5 (a) An ideal dipole with balanced currents, (b) a dipole with unbalanced currents caused by coaxial line.

path A is equal to that of path B. Thus, V^+ and V^- cancel each other out, leading to a zero voltage at point C.

For the welding design, all of the driven elements and parasitic elements should be connected by metal branches. Point C is chosen as the position for connecting the branch, as shown in Fig. 3b. The current on the connector branch consists of the conducted current I_f and the coupling current I_c, where I_f is directly conducted from the WHEMS antenna through point C. As the voltage at point C is zero, the voltage is zero at any point along the branch. Thus, I_f is zero. Current I_c is coupled to the WHEMS by an electromagnetic wave. As shown in Fig. 2, the electric field generated by the currents is perpendicular to the branch; thus, no currents are excited, and I_c is zero. The performance of the WHEMS is not affected by the lack of current in the connector branch. As the entire procedure is based on the structural symmetry and is not limited by the frequency, a gain over wide band can be achieved.

Figure 4 shows a simplified model of a parasitic element with a connector branch, which is excited by the incident wave generated by the WHEMS. The rod is parallel to the WHEMS, with both of their centers in the YOZ plane. As the rod is parallel to the normal vector of the magnetic field, current I_1 is excited by the incident wave. The current along the connector branch, represented as I_2, consists of the conducted element and coupled element, represented as I_{c2} and I_{f2}, respectively. Current I_{c2} on the branch is directly conducted from the rod through its central point. As shown in Fig. 4, the incident wave excites voltages of V^+ and V^- at the rod ends, which have the same amplitude but a phase difference of 180 degrees. Thus, the voltage at an intermediate point on the rod is zero, resulting in a zero voltage anywhere along the branch. Hence, I_{f2} is zero. As the normal vector of the magnetic field is perpendicular to the branch, I_{c2} is zero based on Maxwell's equations. The performance of the parasitic element is not influenced because the connector branch has no current, resulting in wide-band performance.

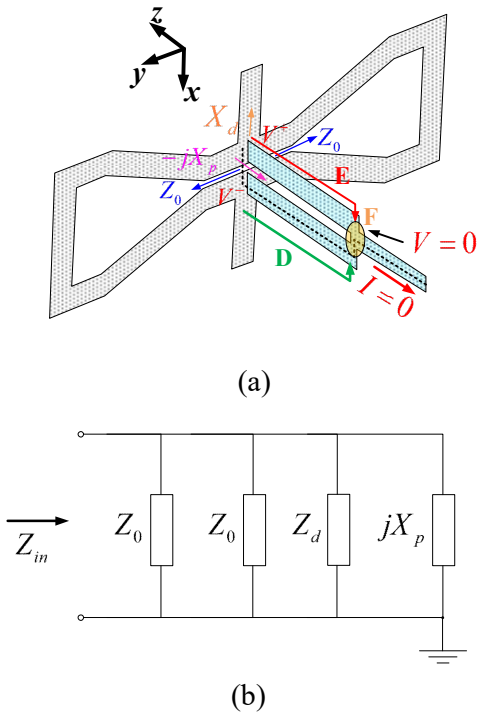

Fig. 6 (a) The balun analysis of the WHEMS. (b) The impedance analysis of the whole driven element.

C. *Voltage Balun*

Any imbalance at the feeding point not only degrades the performance of the antenna, but also increases the noise in the system, triggering radio interference problems. Fig. 5a shows a dipole antenna fed by an ideal lumped port, which is a balanced case. In this case, I_{b1} equals I_{b2}, and the dipole antenna operates in the appropriate state. Fig. 5b shows an unbalanced case, where the antenna is fed by a coaxial line. As shown in the figure, part of I_{b2} flows along the outer layer of the shield, represented as I_{b3}. Hence, I_{b1} no longer equals I_{b2}, leading to a reduction in radiating performance. Moreover, I_{b3} may flow directly to the radio system, leading to noise coupling issues.

To solve the problem, a voltage balun is introduced. As shown in Fig. 6a, the balun, represented as a blue shadow, is directly connected at the feeding point of the WHEMS, which can also be recognized as the shield of a coaxial line. The black dashed line is the signal line inside the shield, the end of which is connected to the top region of the antenna. The signal is transmitted to the WHEMS along the black dashed line inside the shield. Voltages V^+ and V^-, with the same amplitude and opposite phases, are excited at the feed point of the antenna. Paths E and D follow the outer layer of the shield with the same length. Because the voltage is cancelled, the voltage at point F is zero. Thus, I, the unbalanced common mode current, equals zero, which is suitable for wide-band performance.

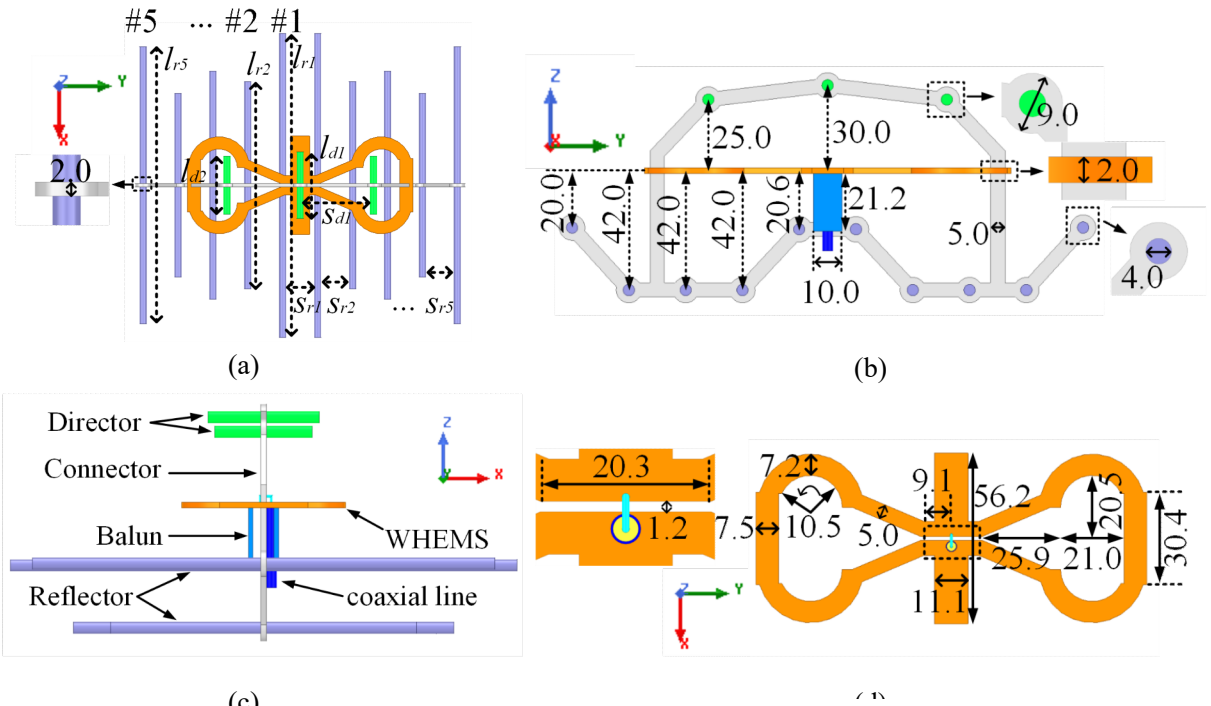

Fig. 7 The configuration of the proposed antenna. (a) The front view; (b) the t millimeters).

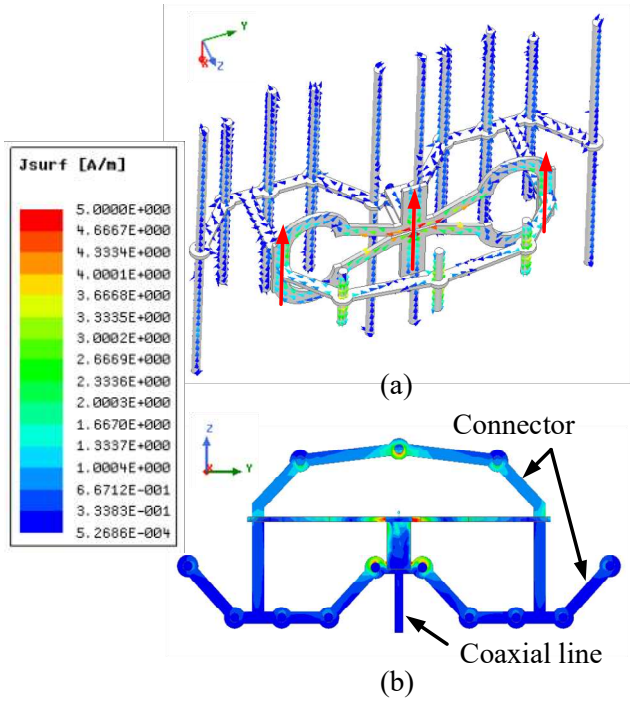

Fig. 8 The current distributions on the antenna at 2.7 GHz, (a) current vector distribution, (b) current amplitude distribution.

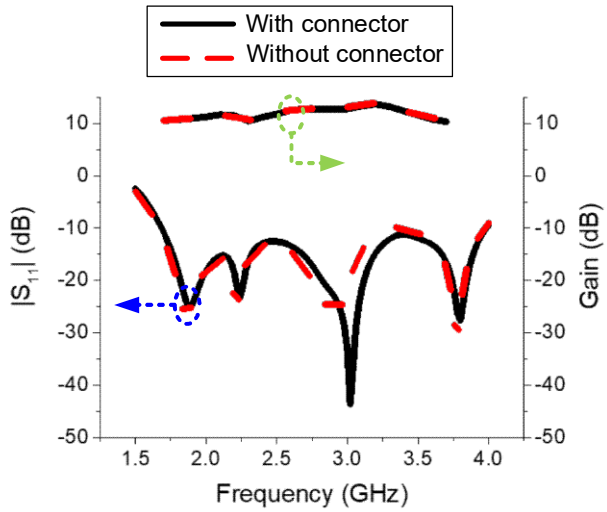

Fig. 9 The $|S_{11}|$ and the gain of the proposed antenna in cases of with connector and without connector.

The balun solves the imbalance arising from the radiation problem and introduces an imaginary component to the input impedance of the WHEMS. As shown in Fig. 6a, the impedance consists of the impedance of the slot loop (Z_0), the dipole (Z_d), and the balun (jX_p), which are connected in parallel with each other. The circuit model is shown in Fig. 6b, with the impedance given by

$$Z_{in} = \frac{Z_0}{2} // Z_d // jX_p \ . \qquad (2)$$

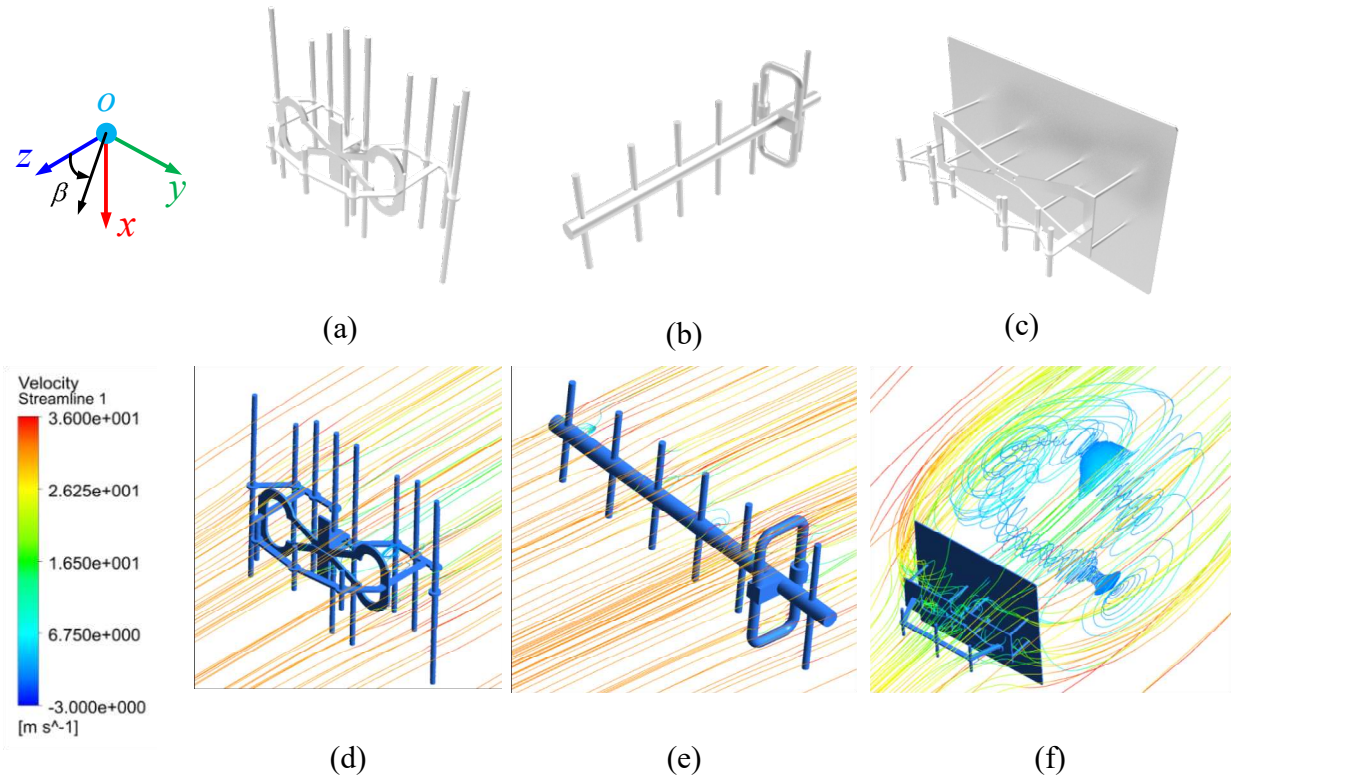

Fig. 10 (a) The model of the proposed antenna, (b) the model of the classical Yagi antenna, (c) the model of the antenna in ref [46], (d) the wind streamline of the proposed antenna, when β is 0 degree, (e) the wind streamline of the classic Yagi antenna, when β is 90 degree, (f) the wind streamline of the antenna in ref [46], when β is 0 degree.

III. Electromagnetic Analysis

Fig. 7 illustrates the configuration of the proposed antenna. It consists of a WHEMS, a director of three rods, a reflector of ten rods, and a balun. The balun has two arms parallel to each other, with one end differentially connected to the WHEMS and the other end short circuited. The antenna is fed by a coaxial line perpendicular to the WHEMS, with the outer layer of the shield connected to one arm of the balun. Both the driven elements and the parasitic elements are linked by a metal connector. The connector is attached to the balun at its short circuit point. The antenna parameters are given in Fig. 7, where $l_{r1}=173.7$ mm, $l_{r2}=118.5$ mm, $l_{r3}=130.5$ mm, $l_{r4}=105.0$ mm, $l_{r5}=158.4$ mm, $S_{r1}=20.0$ mm, $S_{r2}=20.0$ mm, $S_{r3}=20.0$ mm, $S_{r4}=20.0$ mm, and $S_{r5}=20.0$ mm.

Fig. 8a shows the current vector distribution of the antenna at 2.7 GHz, which is accordant with the theoretic model shown in Fig. 2. The current amplitude distribution at 2.7 GHz is shown in Fig. 8b. The balun reduces the current on the outer layer of the shield by -12 dB. The ratio of the current on the connector to the current on the WHEMS is less than -9 dB. A residual current on the connector arises due to cross-polarization radiation and imperfections of the balun, although in the theoretical model, the current along the connector is zero. As the residual current is -9 dB, less than the main radiation, and its polarization is normal to the polarization of the equivalent

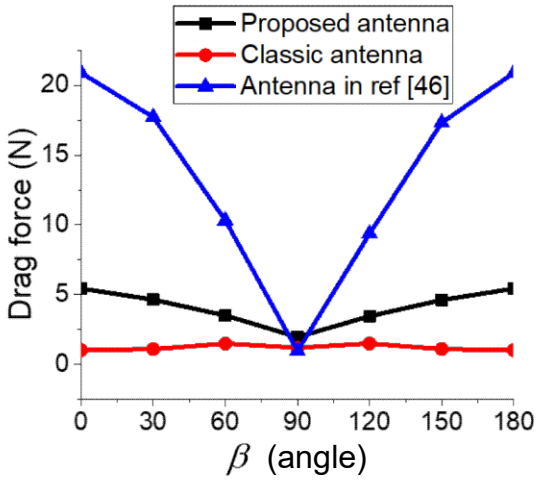

Fig. 11 The drag force of the three antennas in cases of typhoons of force 12 from different orientation angles.

Fig. 12 The photograph of the antenna prototype.

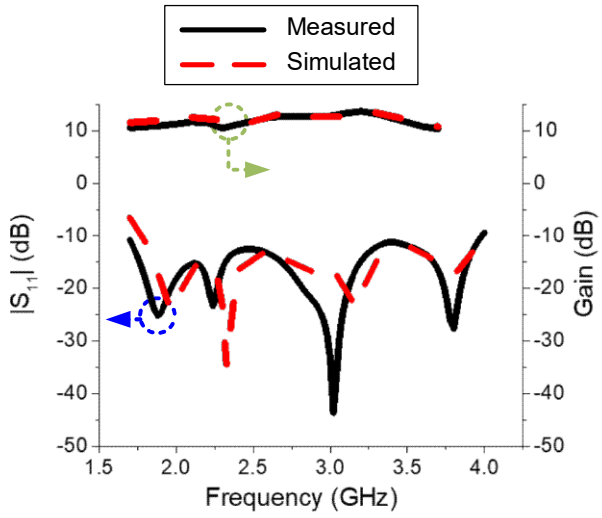

Fig. 13 The measured and simulated |S11| and gain results.

radiating model shown in Fig. 2b, the connector has almost no effect on the radiating performance of the proposed antenna. Fig. 9 shows the $|S_{11}|$ and gain of the proposed antenna for cases with and without a connector respectively based on simulations. The maximum gain variation caused by the connector is less than 0.5 dB in the working band (1.7 GHz to 3.7 GHz). The $|S_{11}|$ curves are accordant with each other, with a value of less than -10 dB in the working band. This result confirms that the connector does not affect the performance of the proposed antenna.

IV. Wind Load Analysis

Wind resistance is a crucial parameter to consider when evaluating the stability of an antenna for an outdoor environment, especially for applications under extreme working conditions. Figs. 10a-c show three simulated models, including the proposed antenna (working over 1.7 GHz to 3.7GHz, with a gain of 12 dBi), the classic Yagi antenna (working over 1.7 GHz to 1.9 GHz, with a gain of 12 dBi), and the antenna in [46] (working over 1.7 GHz to 2.7 GHz, with a gain of 11 dBi). The classic Yagi antenna is representative of a low-wind-resistance antenna, while the antenna in [46], which uses a back plate as the reflector, represents a high-wind-load antenna. Parameter β is the angle of incoming wind in the H-plane (YOZ). The *z*-axis pointing to the radiating directions of the three antennas corresponds to $\beta = 0$. The wind load is simulated using fluent software from ANSYS Co. The wind speed in the simulation is set to 32 m/s, corresponding to the velocity of a typhoon of force 12.

The wind load resistance is calculated by [47]

$$F_D = C_D \times A \times \frac{\rho \times V^2}{2} \tag{3}$$

where F_D, the drag force, is the resultant force of the wind on the antenna, also termed the wind load resistance; V is the speed of the wind flow; ρ is the fluid density; and C_D is the drag coefficient. Coefficient C_D depends on the shape of the object, indicating whether fluid moves around an object in a steady flow or in other flow patterns.

Figs. 10d–f present wind streamlines of the proposed antenna ($\beta = 0$ degrees), the classic Yagi antenna ($\beta = 90$ degrees), and the antenna in [46] ($\beta = 0$ degrees), respectively. Before encountering the three antennas, the wind moves in a steady flow with a speed of 32 m/s. When the wind blows through the proposed antenna and the Yagi antenna, several small vortices of fluid arise, while the flow primarily remains steady. When the wind passes through the antenna in [46], the direction of the wind changes and some larger vortexes appear behind the metal plate. As shown in Fig. 10f, the speed of the vortex decreases to almost zero, which dissipates the energy of the flow. Thus, the pressure behind the plate decreases, which exerts a large drag force on the plate. It can be deduced that the drag force of the antenna in [46] is larger than that of the proposed antenna and the Yagi antenna.

Fig. 11 shows the simulation results for F_D. The maximum F_D of the proposed antenna is 5.4 N when $\beta = 0$ degrees, while the maximum F_D of the Yagi antenna is 1.5 N, which varies slightly with β. The maximum F_D of the antenna in [46] is 20.9 N when $\beta = 0$ degrees, which is 3.9-fold higher than that of the proposed antenna. The F_D results confirm our deduction from the simulated streamline.

V. Results and Discussion

Wind resistance and durability are crucial factors that IoT hardware designers need to consider, especially for the outdoor IoT applications, where the application environment is windy. The proposed antenna can be manufactured through casting or welding process, which makes the antenna more rugged

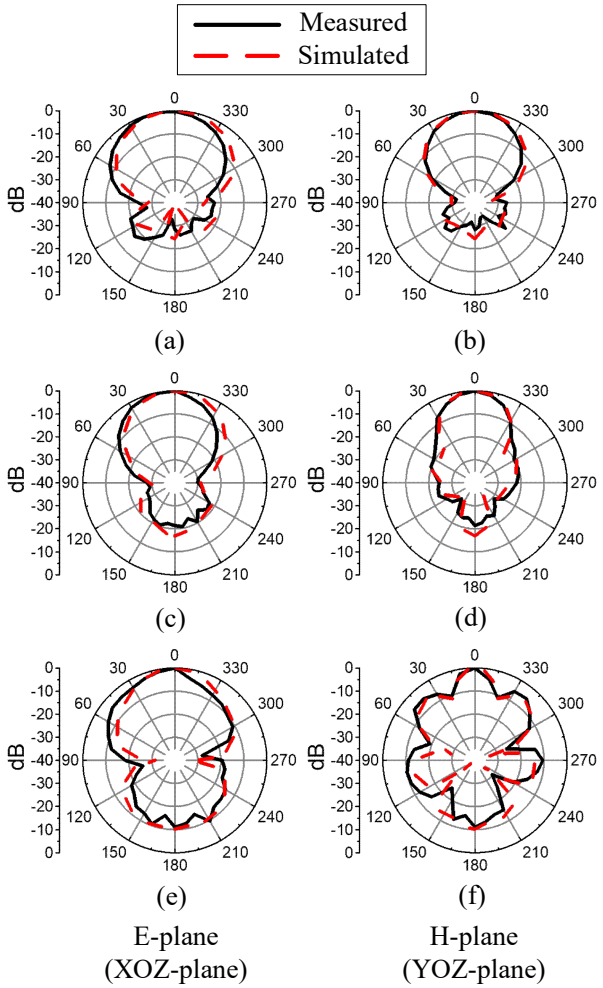

Fig. 14 The measured and simulated patterns in H-plane (YOZ) and E-plane (XOZ) at (a) 1.7 GHz, (b) 2.7 GHz, (c) 3.7GHz.

mechanically. Due to the linear array design, the wind resistance of the antenna is small meeting both ruggedness and low wind resistance ensuring the antenna a fine outdoor performance without a radome.. Fig. 12 shows the fabricated prototype of the newly proposed antenna. The 2D mechanical metal connection part, which has no significant current on it, is the bounding element that joint all of the antenna parts together. In practical applications, the antenna should be manufactured from aluminum alloy, with high strength and light weight; a welding procedure could be applied toin the final production stage. For convenience in the prototype, the antenna was produced from copper, with a soldering procedure applied for assembly. The WHEMS, balun, and connector were manufactured by metal sheet stamping, and the rods were obtained by applying laser cutting to a copper pipe.

The simulated and measured |S11| values are shown in Fig. 13, where good agreement is observed. The simulated and measured -10 dB fractional bandwidth are 80.7% (1.74 GHz) and 75.9% (1.8-4 GHz), respectively, where the measured curve is shifted to higher frequencies by 0.1 GHz as compared with the simulated curve. Fig. 13 also shows the gain results. The measured and simulated gains are 10.8-13.3 dBi and 10.3-13.7 dBi, respectively, for a 74% bandwidth (1.7-3.7 GHz), and the two curves agree well with each other. These wideband and high-gain properties leading to high communication capacity can be used in the current and future IoT applications, such as high-definition video streaming with zero latency reactions. Fig. 14 depicts the pattern results. Again, the simulated patterns agree closely with the measured patterns. The fine directing property proves that the antenna is suitable for nodes communication applications of IoT. The simulated and measured radiation efficiency is shown in Fig. 15. The simulated radiation is 100% in the band, and the measured result is around 90%.The discrepancy in the results are likely due to fabrication errors, assembly errors, and measuring uncertainties, such as errors in the metal sheet stamping process, soldering of the feed point, and the influence of common mode currents on the coaxial line.

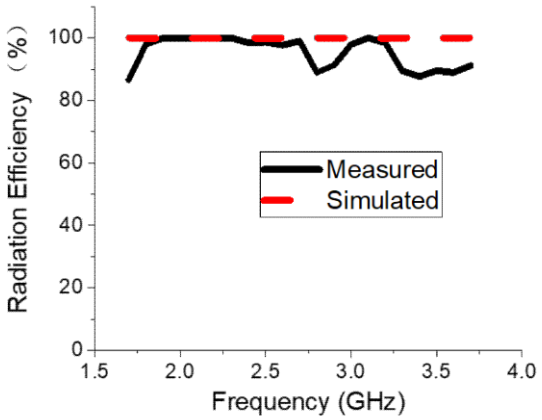

Fig. 15 The simulated and measured results of radiation efficiency.

VI. Conclusion

The antenna mechanical structure devised in the paper is rugged for IoT applications in the outdoor environment, where harsh weather conditions has to be considered. All the parts of the antenna are connected by metal, and with low wind load by using the rods and linear structures. The WHEMS is connected with the rods at the middle point of its both edges enhancing the mechanical strength without sacrificing the electromagnetic performance, where the whole connecting measure is explained in electromagnetic theory and validated in Simulation. The balun, connected to the WHEMS at its feed point and short circuited with the connector, not only chocks the undesired electromagnetic interference to the IoT system but also enhanced the ruggedness of the whole structure ensuring the normal operation of the IoT system under harsh conditions. The whole structure can be finally manufactured through casting or welding. The proposed antenna realized an intermediate gain of 10.8–13.3 dBi for a 78% fractional bandwidth (1.7 GHz – 2.7 GHz), covering both the LTE and 5G sub-6GHz bands. The antenna achieves a four-fold enhanced wind resistance compared to that in [46] with a back plate. The driven element,

reflectors and directors are all metallically connected with all voltage zero points at the centers of its mechanical structure. This electrical design feature makes it possible for weldable rugged mechanical design. With a linear array and metalized design, the antenna not only has a simple feeding arrangement, low cost, light weight, low wind resistance, and rugged structure, similar to the Yagi Uda antenna, but also has a 7-fold greater bandwidth, without sacrificing the gain performance, which is superior to that of a normal log-periodic antenna. Thus, the antenna is a good candidate for all-weather large-scale IoT deployment. Not only the electrical design features of the proposed antenna make the antenna a desired candidate for wide area of IoT applications, but its design principle can be applied to a versatile application scenario such as TV reception and Radar applications.

REFERENCES

[1] A. Lei, H. Cruickshank, Y. Cao, P. Asuquo, C. P. A. Ogah and Z. Sun, "Blockchain-Based Dynamic Key Management for Heterogeneous Intelligent Transportation Systems," *IEEE Internet Things J.*, vol. 4, no. 6, pp. 1832-1843, Dec. 2017.

[2] E. Sisinni, A. Saifullah, S. Han, U. Jennehag and M. Gidlund, "Industrial Internet of Things: Challenges, Opportunities, and Directions," *IEEE Trans. Ind. Informat.*, vol. 14, no. 11, pp. 4724-4734, Nov. 2018.

[3] N. Ahmed, D. De and I. Hussain, "Internet of Things (IoT) for Smart Precision Agriculture and Farming in Rural Areas," *IEEE Internet Things J.*, vol. 5, no. 6, pp. 4890-4899, Dec. 2018.

[4] H. Zhang, J. Li, B. Wen, Y. Xun and J. Liu, "Connecting Intelligent Things in Smart Hospitals Using NB-IoT," *IEEE Internet Things J.*, vol. 5, no. 3, pp. 1550-1560, June 2018.

[5] R. M. González, F. D. Wattjes, M. Gibescu, W. Vermeiden, J. G. Slootweg and W. L. Kling, "Applied Internet of Things Architecture to Unlock the Value of Smart Microgrids," *IEEE Internet Things J.*, vol. 5, no. 6, pp. 5326-5336, Dec. 2018.

[6] G. Bedi, G. K. Venayagamoorthy, R. Singh, R. R. Brooks and K. Wang, "Review of Internet of Things (IoT) in Electric Power and Energy Systems," *IEEE Internet Things J.*, vol. 5, no. 2, pp. 847-870, April 2018.

[7] Y. Li, X. Cheng, Y. Cao, D. Wang and L. Yang, "Smart Choice for the Smart Grid: Narrowband Internet of Things (NB-IoT)," *IEEE Internet Things J.*, vol. 5, no. 3, pp. 1505-1515, June 2018.

[8] S. Dong, S. Duan, Q. Yang, J. Zhang, G. Li and R. Tao, "MEMS-Based Smart Gas Metering for Internet of Things," *IEEE Internet Things J.*, vol. 4, no. 5, pp. 1296-1303, Oct. 2017.

[9] Y. Yao, Y. Sun, C. Phillips and Y. Cao, "Movement-Aware Relay Selection for Delay-Tolerant Information Dissemination in Wildlife Tracking and Monitoring Applications," *IEEE Internet Things J.*, vol. 5, no. 4, pp. 3079-3090, Aug. 2018.

[10] Y. Yao, Y. Sun, C. Phillips, Y. Cao and J. Li, "Exploiting Delay Budget Flexibility for Efficient Group Delivery in the Internet of Things," *IEEE Internet Things J.*, vol. 6, no. 4, pp. 6593-6605, Aug. 2019.

[11] Z. Lv, B. Hu and H. Lv, "Infrastructure Monitoring and Operation for Smart Cities based on IoT system," *IEEE Trans Ind. Informat.*.

[12] Y. Zhong, E. Dutkiewicz, Y. Yang, X. Zhu, Z. Zhou and T. Jiang, "Internet of Mission-Critical Things: Human and Animal Classification—A Device-Free Sensing Approach," *IEEE Internet Things J.*, vol. 5, no. 5, pp. 3369-3377, Oct. 2018.

[13] F. Zhang, M. Liu, Z. Zhou and W. Shen, "An IoT-Based Online Monitoring System for Continuous Steel Casting," *IEEE Internet Things J.*, vol. 3, no. 6, pp. 1355-1363, Dec. 2016.

[14] M. Jin, X. Zhou, E. Luo and X. Qing, "Industrial-QoS-Oriented Remote Wireless Communication Protocol for the Internet of Construction Vehicles," *IEEE Trans. Ind. Electron*., vol. 62, no. 11, pp. 7103-7113, Nov. 2015.

[15] Q. Chi, H. Yan, C. Zhang, Z. Pang and L. D. Xu, "A Reconfigurable Smart Sensor Interface for Industrial WSN in IoT Environment," *IEEE Trans Ind. Informat.*, vol. 10, no. 2, pp. 1417-1425, May 2014.

[16] M. E. E. Alahi, L. Xie, S. Mukhopadhyay and L. Burkitt, "A Temperature Compensated Smart Nitrate-Sensor for Agricultural Industry," *IEEE Trans. Ind. Electron*., vol. 64, no. 9, pp. 7333-7341, Sept. 2017.

[17] Hwaiyu Geng, "IoT REVOLUTION IN OIL AND GAS INDUSTRY," in *Internet of Things and Data Analytics Handbook* , Wiley, 2017.

[18] G. Yang *et al*., "A Health-IoT Platform Based on the Integration of Intelligent Packaging, Unobtrusive Bio-Sensor, and Intelligent Medicine Box," *IEEE Trans Ind. Informat.*, vol. 10, no. 4, pp. 2180-2191, Nov. 2014.

[19] A. Zanella, N. Bui, A. Castellani, L. Vangelista and M. Zorzi, "Internet of Things for Smart Cities," *IEEE Internet Things J.*, vol. 1, no. 1, pp. 22-32, Feb. 2014.

[20] J. A. Stankovic, "Research Directions for the Internet of Things," *IEEE Internet Things J.*, vol. 1, no. 1, pp. 3-9, Feb. 2014.

[21] S. Chen, H. Xu, D. Liu, B. Hu and H. Wang, "A Vision of IoT: Applications, Challenges, and Opportunities With China Perspective," *IEEE Internet Things J.*, vol. 1, no. 4, pp. 349-359, Aug. 2014.

[22] E. Hegland Hjort Kure, P. Engelstad, S. Maharjan, S. Gjessing and Y. Zhang, "Distributed Uplink Offloading for IoT in 5G Heterogeneous Networks Under Private Information Constraints," *IEEE Internet Things J.*, vol. 6, no. 4, pp. 6151-6164, Aug. 2019.

[23] M. Vilgelm, S. Rueda Liñares and W. Kellerer, "Dynamic Binary Countdown for Massive IoT Random Access in Dense 5G Networks," *IEEE Internet Things J.*, vol. 6, no. 4, pp. 6896-6908, Aug. 2019.

[24] H. Yagi and S. Uda, "Projector of the sharpest beam of electric waves," *Proc. Imperial Acad.,* vol. 2, pp. 49–52, Feb. 1926.

[25] D. M. Pozar, "Beam Transmission Of Ultra Short Waves: An Introduction To The Classic Paper By H. Yagi," Proc. IEEE, vol. 85, no. 11, pp. 1857-1863, Nov. 1997.

[26] Raad, Haider . "A Yagi-Uda antenna array for conformal IoT and wireless charging applications," *Microw. Opt. Tech. Lett.*(2018).

[27] C. Lee and Liang-Chi Shen, "Coupled Yagi arrays," in IEEE Transactions on Antennas and Propagation, vol. 25, no. 6, pp. 889-891, November 1977..

[28] T. Kosako, Y. Kadoya, H. F. Hofmann . "Optical antennas direct single-molecule emission" *Nature Photon*, vol. 2, pp.234–237, Mar. 2008.

[29] Giessen, H. , and M. Lippitz . "Directing Light Emission from Quantum Dots." *Science*, vol. 329, pp. 910-911, 2010.

[30] Curto, A. G. , et al. "Unidirectional Emission of a Quantum Dot Coupled to a Nanoantenna." *Science*, vol. 329, pp. 930-933 2010.

[31] Y. Qian, W. R. Deal, N. Kaneda and T. Itoh, "Microstrip-fed quasi-Yagi antenna with broadband characteristics," *Electron. Lett.*, vol. 34, no. 23, pp. 2194-2196, 12 Nov. 1998.

[32] N. Kaneda, Y. Qian and T. Itoh, "A broad-band microstrip-to-waveguide transition using quasi-Yagi antenna," *IEEE Trans. Microw. Theory Tech.,* vol. 47, no. 12, pp. 2562-2567, Dec. 1999.

[33] W. R. Deal, N. Kaneda, J. Sor, Y. Qian and T. Itoh, "A new quasi-Yagi antenna for planar active antenna arrays," *IEEE Trans. Microw. Theory Tech.*, vol. 48, no. 6, pp. 910-918, June 2000.

[34] J. Yeo and J. Lee, "Bandwidth Enhancement of Double-Dipole Quasi-Yagi Antenna Using Stepped Slotline Structure," *IEEE Antennas Wireless Propag. Lett.*, vol. 15, pp. 694-697, 2016.

[35] N. Kaneda, W. R. Deal, Yongxi Qian, R. Waterhouse and T. Itoh, "A broadband planar quasi-Yagi antenna," *IEEE Trans. Antennas Propag.*, vol. 50, no. 8, pp. 1158-1160, Aug. 2002.

[36] N. A. Bishop, J. Miller, D. Zeppettella, W. Baron, J. Tuss and M. Ali, "A Broadband High-Gain Bi-Layer LPDA for UHF Conformal Load-Bearing Antenna Structures (CLASs) Applications," *IEEE Trans. Antennas Propag.*, vol. 63, no. 5, pp. 2359-2364, May 2015.

[37] K. Anim and Y. Jung, "Shortened Log-Periodic Dipole Antenna Using Printed Dual-Band Dipole Elements," *IEEE Trans. Antennas Propag.*, vol. 66, no. 12, pp. 6762-6771, Dec. 2018.

[38] Q. Wu, R. Jin and J. Geng, "A Single-Layer Ultrawideband Microstrip Antenna," *IEEE Trans. Antennas Propag.*, vol. 58, no. 1, pp. 211-214, Jan. 2010.

[39] P. Fei, Y. Qi and Y. Jiao, "Design of a Wideband Dual-Element Slot Loop Antenna Array With Adjustable Back-Reflector," *IEEE Antennas Wireless Propag. Lett.*, vol. 11, pp. 1014-1017, 2012.

[40] W. Liang, Y. Qi and Y. Jiao, "A Novel Small Director Array for Slot Loop Antenna for LTE Application," *IEEE Antennas Wireless Propag. Lett.*, vol. 12, pp. 1110-1113, 2013.

[41] X. Gao, Y. Qi and Y. Jiao, "Design of Multiplate Back-Reflector for a Wideband Slot Antenna," *IEEE Antennas Wireless Propag. Lett.*, vol. 12, pp. 773-776, 2013.

[42] H. Wen, Y. Qi, Z. Weng, F. Li and J. Fan, "A Multiband Dual-Polarized

Omnidirectional Antenna for 2G/3G/LTE Applications," *IEEE Antennas Wireless Propag. Lett.*, vol. 17, no. 2, pp. 180-183, Feb. 2018.

[43] L. Chi, Y. Qi, Z. Weng, W. Yu, F. Li and J. L. Drewniak, "Directional Antenna With Consistent H-Plane Dual-Band Beamwidth for Wi-Fi Applications," *IEEE Trans. Antennas Propag.*, vol. 67, no. 7, pp. 4495-4505, July 2019.

[44] Y. Xiao, Y. Qi, F. Li, J. Fan, W. Yu and L. Lu, "Dual-Band Directional Slot Antenna for Wi-Fi Application," *IEEE Trans. Antennas Propag.*, vol. 66, no. 8, pp. 4277-4281, Aug. 2018.

[45] Z. Cai, Y. Qi, Z. Weng, W. Yu, F. Li and J. Fan, "DC ground compact wideband omnidirectional vertically polarised slot loop antenna for 4G long-term evolution applications," *IET Microw., Antennas & Propag.*, vol. 12, no. 7, pp. 1087-1092, 13 6 2018.

[46] L. Chi, Y. Qi, Z. Weng, W. Yu and W. Zhuang, "A Compact Wideband Slot-Loop Directional Antenna for Marine Communication Applications," *IEEE Trans. Veh. Technol.*, vol. 68, no. 3, pp. 2401-2412, March 2019.

[47] J. D. Anderson, Jr., *Fundamentals of Aerodynamics,* 5nd ed. New York: McGraw-Hill, 2007.